

## Article

# Green Synthesis and Antibacterial Activity of Ag/Fe<sub>2</sub>O<sub>3</sub> Nanocomposite Using *Buddleja lindleyana* Extract

Fatimah A. M. Al-Zahrani <sup>1,\*</sup>, Salem S. Salem <sup>2,\*</sup>, Huda A. Al-Ghamdi <sup>3</sup>, Laila M. Nhari <sup>3</sup>, Long Lin <sup>4</sup>  
and Reda M. El-Shishtawy <sup>5,6,\*</sup>

- <sup>1</sup> Chemistry Department, Faculty of Science, King Khalid University, Abha 61413, Saudi Arabia  
<sup>2</sup> Botany and Microbiology Department, Faculty of Science, Al-Azhar University, Cairo 11884, Egypt  
<sup>3</sup> Chemistry Department, Faculty of Science, University of Jeddah, Jeddah 21959, Saudi Arabia  
<sup>4</sup> Colour Science, School of Chemistry, University of Leeds, Woodhouse Lane, Leeds LS2 9JT, UK  
<sup>5</sup> Chemistry Department, Faculty of Science, King Abdulaziz University, Jeddah 21589, Saudi Arabia  
<sup>6</sup> Dyeing, Printing and Textile Auxiliaries Department, Institute of Textile Research and Technology, National Research Centre, 33 EL Buhouth St., Dokki, Giza 12622, Egypt  
\* Correspondence: falzhrani@kku.edu.sa (F.A.M.A.-Z.); salemsalahsalem@azhar.edu.eg (S.S.S.); relshishtawy@kau.edu.sa (R.M.E.-S.)

**Abstract:** In the study reported in this manuscript, silver/iron oxide nanocomposites (Ag/Fe<sub>2</sub>O<sub>3</sub>) were phytosynthesized using the extract of *Buddleja lindleyana* via a green, economical and eco-friendly strategy. The biosynthesized Ag/Fe<sub>2</sub>O<sub>3</sub> nanocomposites were characterized using UV-Vis spectrophotometry, FTIR, XRD, TEM, DLS and SEM-EDX analyses. The particulates showed a triangular and spherical morphology having sizes between 25 and 174 nm. FTIR studies on the nanoparticles showed functional groups corresponding to organic metabolites, which reduce and stabilize the Ag/Fe<sub>2</sub>O<sub>3</sub> nanocomposite. The antimicrobial efficacy of the phytosynthesized Ag/Fe<sub>2</sub>O<sub>3</sub> against bacterial pathogens was assessed. In addition, Ag/Fe<sub>2</sub>O<sub>3</sub> exhibited broad spectrum activities against *B. subtilis*, *S. aureus*, *E. coli*, and *P. aeruginosa* with inhibition zones of 23.4 ± 0.75, 22.3 ± 0.57, 20.8 ± 1.6, and 19.5 ± 0.5 mm, respectively. The Ag/Fe<sub>2</sub>O<sub>3</sub> composites obtained showed promising antibacterial action against human bacterial pathogens (*S. aureus*, *E. coli*, *B. subtilis* and *P. aeruginosa*), making them candidates for medical applications.

**Keywords:** *Buddleja lindleyana*; Ag/Fe<sub>2</sub>O<sub>3</sub>; nanocomposite; phytosynthesis; antimicrobial activity



**Citation:** Al-Zahrani, F.A.M.; Salem, S.S.; Al-Ghamdi, H.A.; Nhari, L.M.; Lin, L.; El-Shishtawy, R.M. Green Synthesis and Antibacterial Activity of Ag/Fe<sub>2</sub>O<sub>3</sub> Nanocomposite Using *Buddleja lindleyana* Extract. *Bioengineering* **2022**, *9*, 452. <https://doi.org/10.3390/bioengineering9090452>

Academic Editors: Hirak Patra and Suryyani Deb

Received: 20 August 2022

Accepted: 5 September 2022

Published: 8 September 2022

**Publisher's Note:** MDPI stays neutral with regard to jurisdictional claims in published maps and institutional affiliations.



**Copyright:** © 2022 by the authors. Licensee MDPI, Basel, Switzerland. This article is an open access article distributed under the terms and conditions of the Creative Commons Attribution (CC BY) license (<https://creativecommons.org/licenses/by/4.0/>).

## 1. Introduction

In recent years, leaf extract-mediated biosynthesis of nanomaterials has been extensively studied [1–4]. Leaf extract-mediated synthesis of nanomaterials is more eco-friendly and economical than other methods of synthesis such as chemical reduction and physical methods [5–7]. Due to the growing demand for ecologically friendly material synthesis techniques, the biosynthesis of nanomaterials has gained attention as an emerging feature of the interface of nanotechnology and biotechnology [8–17]. The biosynthesis of inorganic materials, particularly metal nanoparticles, utilizing microbes and plants has received a lot of attention [18–24]. Nanosilver has many important applications [25–28]. Antimicrobial agents have been utilized with it [29,30]. The study reported in the first paper on green leaf cell extract solution-mediated synthesis of Ag/Fe<sub>2</sub>O<sub>3</sub> hybrid nanoparticles successfully employed a green method to synthesize Fe<sub>2</sub>O<sub>3</sub> as well as Ag/Fe<sub>2</sub>O<sub>3</sub> nanoparticles. The synthesized nanoparticles showed excellent antibacterial, antifungal and anticancer activities [31]. Utilizing various reducing agents as well as no reducing agents, it was successful to produce nano-hybrid Ag/Fe<sub>2</sub>O<sub>3</sub>NPs depending on carboxymethyl-chitosan. Their fairly reversible magnetization curves show that γ-Fe<sub>2</sub>O<sub>3</sub> NPs transition to a superparamagnetic state [32]. Antibacterial testing on nanocomposites revealed good antimicrobial action against both Gram-positive and Gram-negative bacteria, as well as good activity

against yeast and *S. aureus* resistant strain [33]. The Ag/Fe<sub>2</sub>O<sub>3</sub>-Graphene oxide (GO) nanocomposites have shown superior long-term antibacterial capabilities against bacteria (Gram-negative and Gram-positive bacteria), demonstrating their particular potential as a promising long-term biocide with minimal environmental hazard. These abilities were compared to plain Ag nano and Ag/Fe<sub>2</sub>O<sub>3</sub> [34]. The creation of Ag on magnetic-Fe<sub>3</sub>O<sub>4</sub> NPs surfaces modified using *Stachys lavandulifolia* extract as a reducing and stabilizing magnetic agent was proposed as an effective and environmentally friendly method. Furthermore, the 4-nitrophenol reduction using the nanocomposite and its bactericidal activity was evaluated [35]. Nanocomposites such as Fe<sub>3</sub>O<sub>4</sub> or Ag/Fe<sub>2</sub>O<sub>3</sub> are covered by porous silica oxides serving as magnetic cores to carry anticancer drugs [36]. Nanomaterials which have magnetic behavior, such as Fe<sub>3</sub>O<sub>4</sub> or Ag/Fe<sub>2</sub>O<sub>3</sub>, are good candidates for superparamagnetism [37,38]. Magnetic resonance imaging (MRI) investigations also utilize iron oxide nanoparticles [39]. The combination of Ag and Fe<sub>2</sub>O<sub>3</sub> achieves the properties of both metals [40]. Due to these properties, researchers have been interested in making a hybrid composite of Ag/Fe<sub>2</sub>O<sub>3</sub> offering better catalytic, bactericidal, and bio-imaging properties [41–43]. To prepare metal nanoparticles, different techniques such as physicochemical, chemical, and green synthesis by using plant, algae, fungi, and bacterial extracts can be employed [44–55]. Plant-based NPs are highly active against different epidemic microbial diseases and are nontoxic to humans [56,57]. The easiest method to synthesize Ag/Fe<sub>2</sub>O<sub>3</sub> nanocomposite by utilizing *Algaia Monozyga* extract as a natural reducing and capping agent was studied [41]. Numerous experimenters have utilized *Rumix acetosa*, *Hordeum vulgare*, and *Azadiracta indica* in the green fabrication of Fe<sub>2</sub>O<sub>3</sub>NPs [58,59]. Leaf extract-mediated synthesis of Fe<sub>2</sub>O<sub>3</sub>NPs is gaining the attention of researchers because of its lower toxicity compared to other chemical reduction methods [28]. Due to their potential utility in targeted drug administration and magnetic hyperthermia cancer treatment, extensive study has been completed on the anticancer properties of Fe<sub>2</sub>O<sub>3</sub>NPs [60–63]. There have been very few reports of investigations on the creation of Ag/Fe<sub>2</sub>O<sub>3</sub> NPs. According to Chen et al., several heteromers of Ag/Fe<sub>2</sub>O<sub>3</sub> NPs may be synthesized and exhibit bactericidal properties [43]. It is hypothesized that a key factor in the antibacterial action of Ag/Fe<sub>2</sub>O<sub>3</sub> NPs is the release of Ag<sup>+</sup> ions [41]. Pathogens including bacteria and fungus, which are multi-drug-resistant pathogens, are more easily defeated by Ag/Fe<sub>2</sub>O<sub>3</sub> NPs than by Ag NPs alone. To the best of our knowledge, this is the first publication to examine the biosynthesis of the Ag/Fe<sub>2</sub>O<sub>3</sub> by *Buddleja lindleyana* leaves. The present study aims to study the green synthesis of nanocomposite Ag/Fe<sub>2</sub>O<sub>3</sub> NPs-based safe natural *Buddleja lindleyana* leaves as a capping and reducing agent. Additionally, the impact of Ag/Fe<sub>2</sub>O<sub>3</sub> NPs on harmful bacteria was investigated.

## 2. Materials and methods

### 2.1. Materials

*Buddleja lindleyana* leaves were collected in the UK. Fe<sub>2</sub>(SO<sub>4</sub>)<sub>3</sub>·6H<sub>2</sub>O and silver nitrate (AgNO<sub>3</sub>, >99.98%) were purchased from Sigma-Aldrich. All aqueous solutions were prepared using distilled deionized (DI) water.

### 2.2. Biosynthesis of Ag/Fe<sub>2</sub>O<sub>3</sub>

Firstly, *Buddleja lindleyana* leaves were carefully washed with DI water to remove impurity and then dried for 2 days at room temperature. The *Buddleja lindleyana* leaves were then weighed out at 10 g and added to 100 mL of DI water. After being heated for 30 min at 90 °C, the mixture was filtered to filter out the broth [31]. The final extract was collected for further usage. For the synthesis of Ag/Fe<sub>2</sub>O<sub>3</sub>, a suitable aqueous solution of *Buddleja lindleyana* extract was gradually added into the mixture containing 1 g Fe(SO<sub>4</sub>)<sub>3</sub>·6H<sub>2</sub>O and 0.1 g silver nitrate (AgNO<sub>3</sub>) in an Erlenmeyer flask while stirring at 300 rpm with a magnetic stirrer at 70 °C for 3 h.

### 2.3. Characterization of Ag/Fe<sub>2</sub>O<sub>3</sub>

Preliminary characterization of the Ag/Fe<sub>2</sub>O<sub>3</sub> prepared was carried out using UV-Vis spectroscopy. The measurement was carried out using a Jasco dual-beam spectrophotometer (model V-530, Tokyo, Japan) having an operational wavelength range of 300 to 800 nm. Thereafter, the formed pellet was used to identify functional groups present using FTIR spectroscopy. In addition, FTIR was employed to identify the functional groups present in the aqueous leaf extract that led to the formation of nanocomposite. For that, the dry leaf powder of *Buddleja lindleyana* was pelletized, and their FTIR (Jasco 460 plus, Tokyo, Japan) spectra were recorded between 4000 and 400 cm<sup>-1</sup>. UV-Vis spectroscopy was used to perform preliminary characterization of the Ag/Fe<sub>2</sub>O<sub>3</sub> produced. With an operating wavelength range of 300 to 800 nm, the measurement was performed using a Jasco dual-beam spectrophotometer (model V-530, Tokyo, Japan). The produced pellet was then utilized to analyze the functional groups using FTIR spectroscopy. Additionally, FTIR was used to pinpoint the functional groups in the aqueous leaf extract that contributed to the creation of the nanocomposite. In order to do that, pellets of *Buddleja lindleyana*'s dry leaf powder were made, and their FTIR (Jasco, 460-plus, Tokyo, Japan) spectra were taken between 4000 and 400 cm<sup>-1</sup>. The FTIR spectra for *Buddleja lindleyana* extract and the spectrum for the aqueous extract of Ag/Fe<sub>2</sub>O<sub>3</sub> were assembled. The size and morphological characterization of the synthesized and lyophilized Ag/Fe<sub>2</sub>O<sub>3</sub> was assessed using transmission electron microscope (TEM). TEM (JEOL-1010, Tokyo, Japan) was used to describe Ag/Fe<sub>2</sub>O<sub>3</sub> in order to determine their sizes and morphologies. The outcome was obtained by injecting the carbon-coated copper grid with Ag/Fe<sub>2</sub>O<sub>3</sub> solution and placing it on a sample holder. Furthermore, the X-ray thin film diffraction measurement for the bio-reduced Ag/Fe<sub>2</sub>O<sub>3</sub> was also performed using a Goniometer = PW3050/60 using Cu K $\alpha$  radiation at 40 kV and 25 °C. Subsequently, relevant X-ray patterns were obtained in the range of 20–80 °C. DLS (dynamic light scattering) particle sizing was employed to study the dispersion of Ag/Fe<sub>2</sub>O<sub>3</sub> in colloidal utilizing the Zetasizer Nanosizer (Malvern-Instruments, Worcestershire, UK). For the particle size analysis, the Ag/Fe<sub>2</sub>O<sub>3</sub> sample was re-suspended in purified water at 25 ppm and vortex-mixed to obtain a homogenous solution. A field emission scanning electron microscope (FESEM) (Quanta, 250-FEG, Taipei, Taiwan) was connected to an energy-dispersive X-ray analyzer (EDX, Unit). EDX and mapping were used to determine the surfaces of the prepared Ag/Fe<sub>2</sub>O<sub>3</sub>.

### 2.4. Assessment of the Inhibitory Activity of Ag/Fe<sub>2</sub>O<sub>3</sub> against Pathogenic Microbes

The inhibitory activity of the Ag/Fe<sub>2</sub>O<sub>3</sub> against bacteria and fungi was assessed using a well-diffusion test. Four bacteria including *B. subtilis*, *S. aureus*, *E. coli*, and *P. aeruginosa* were employed for the tests. Using the streaking method, test bacteria were inoculated into sterile Petri plates containing 20 mL of Mueller–Hinton. Sterile cork borer (6 mm) was used to prepare wells, and then, 200  $\mu$ L of Ag/Fe<sub>2</sub>O<sub>3</sub> at a concentration of 5 mg/mL was added in the well. The inoculated plates were kept in a refrigerator for 45 min to achieve adequate diffusion of Ag/Fe<sub>2</sub>O<sub>3</sub>, which was followed by incubation at 37 °C for 24 h for the bacteria test. The inhibition zone around each well was measured.

## 3. Results and Discussion

### 3.1. Synthesis of Ag/Fe<sub>2</sub>O<sub>3</sub> Nanoparticles

One of the goals of this study was to use *Buddleja lindleyana* plant sources for the preparation of nanomaterials. The *Buddleja lindleyana* plant, which belongs to the Loganiaceae family, was chosen and used in this study for Ag/Fe<sub>2</sub>O<sub>3</sub> synthesis. The main chemical components of *Buddleja lindleyana* include flavonoids, triterpenoids, phenylethanoids, and iridoid glycosides [64–66]. The primary idea behind this procedure was to develop a clean, environmentally friendly method of creating nanomaterials using *Buddleja lindleyana* extract, which has the ability to function as both a reducing and a stabilizing agent in the production of a Ag/Fe<sub>2</sub>O<sub>3</sub> nanocomposite (Figure 1).

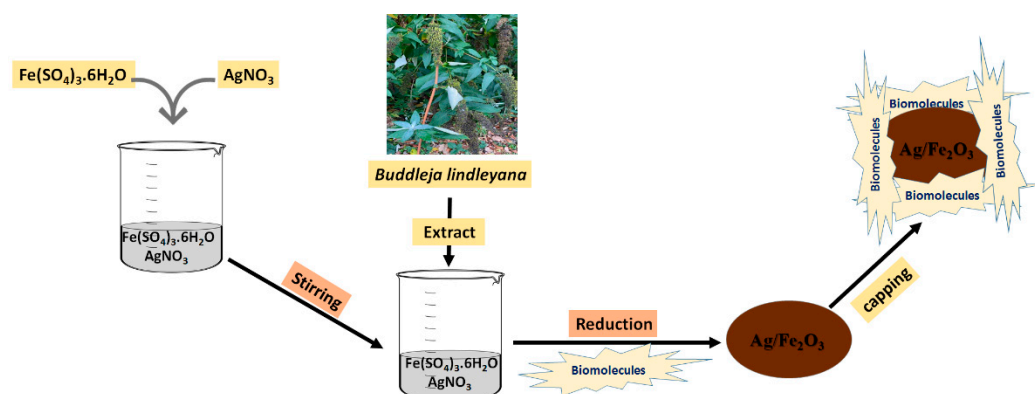


**Figure 1.** The mechanism of the reduction process of the  $\text{Ag}/\text{Fe}_2\text{O}_3$  nanocomposite using *Buddleja lindleyana* extract.

The synthesis of  $\text{Ag}/\text{Fe}_2\text{O}_3$  was conducted by adding  $\text{Fe}(\text{SO}_4)_3 \cdot 6\text{H}_2\text{O}$  and  $\text{AgNO}_3$  as a precursor to the *Buddleja lindleyana* leaf extract until a gradual change in the reaction color was observed. After 3 h of incubation at  $70^\circ\text{C}$ , the color of the reaction mixture changed from pale green to dark brown (Figure 2). Such a change of color of the reaction mixture represents the formation of  $\text{Ag}/\text{Fe}_2\text{O}_3$  by the *Buddleja lindleyana* extract. UV-Vis spectra of the  $\text{Ag}/\text{Fe}_2\text{O}_3$  nanocomposite after 3 h were measured within the range of 300–800 nm and are presented in Figure 2. The strong peak formed at 320 nm, as visible in the UV-Vis spectra, was used to identify the formation of  $\text{Ag}/\text{Fe}_2\text{O}_3$  nanocomposite. Similarly, UV-Vis studies of  $\text{Ag}/\text{Fe}_2\text{O}_3$  NPs by Berastegui et al. revealed high-level absorptions from 300 to 650 nm [67]. The presence of  $\text{Ag}/\text{Fe}_2\text{O}_3$  nanocomposite caused the widening of absorbance at 320 nm (Figure 2).

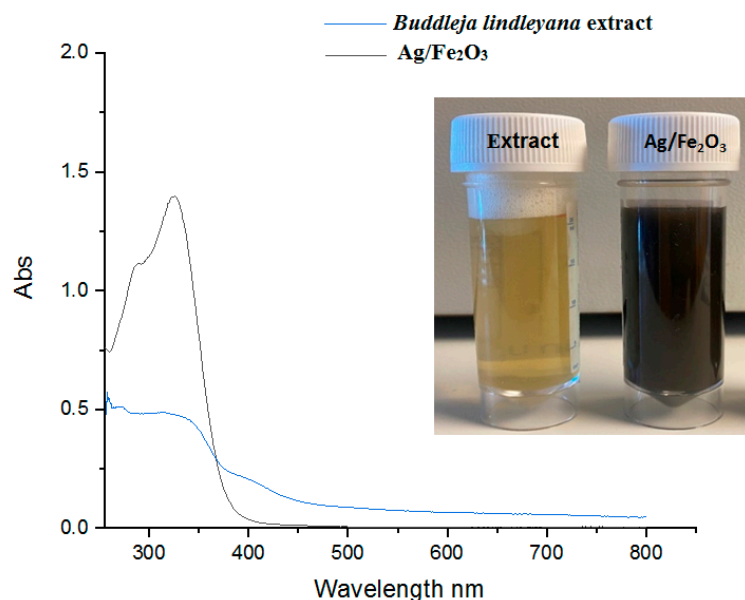


**Figure 2.** Color change and UV-Vis absorption spectra of  $\text{Ag}/\text{Fe}_2\text{O}_3$  nanocomposite synthesis by *Buddleja lindleyana* extract.

FTIR spectroscopic analysis was used to investigate the structural features of the bioactive constituents in *Buddleja lindleyana* extract as well as the probable chemical alterations due to the formation of  $\text{Ag}/\text{Fe}_2\text{O}_3$ . As indicated in Figure 3, the bonding arrangements of *Buddleja lindleyana* were investigated using FTIR in the spectrum range of  $400\text{--}4000\text{ cm}^{-1}$  (Figure 3). The H-bonded and -OH stretch vibrating of hydroxyl and phenolic groups of *Buddleja lindleyana* extract was found in a wide range  $3367.9\text{--}3216.9\text{ cm}^{-1}$  [31]. The -CH

group is responsible for the bands at  $2918.5\text{ cm}^{-1}$  and  $2850.6\text{ cm}^{-1}$ . The presence of C-O of the ester group is indicated by the strong peak seen at  $1728.7\text{ cm}^{-1}$ . The existence of NH amine is shown by the peak at  $1603.8\text{ cm}^{-1}$  [20]. The existence of functional groups such as carboxylic acid and ether is further confirmed by FTIR analysis, which provides a peak value of  $1008\text{ cm}^{-1}$ . The bioactive chemicals in *Buddleja lindleyana* extract are employed to convert ions into their appropriate metal forms. Furthermore, these phytochemicals have extremely reactive hydroxyl groups, which give hydrogen and so help to reduce the quantity of free radicals. The findings support the theory that these phytochemicals play a role in the bio-reduction process that leads to the production of nanomaterials [68,69]. According to the IR spectra of Ag/Fe<sub>2</sub>O<sub>3</sub>, the suppression of aliphatic molecules in Ag/Fe<sub>2</sub>O<sub>3</sub> can be linked to redox changes of phytochemicals during Ag/Fe<sub>2</sub>O<sub>3</sub> formation (Figure 3). Furthermore, IR studies revealed that chemical groups from the extract were bound to the Ag/Fe<sub>2</sub>O<sub>3</sub> layer, indicating that *Buddleja lindleyana* extract worked as a stabilizer for the development of nanocomposite. The bending vibration of AgO and FeO interactions in Ag/Fe<sub>2</sub>O<sub>3</sub> may explain the occurrence of peaks at  $611.4$  and  $561.4\text{ cm}^{-1}$ , respectively, in Figure 3.

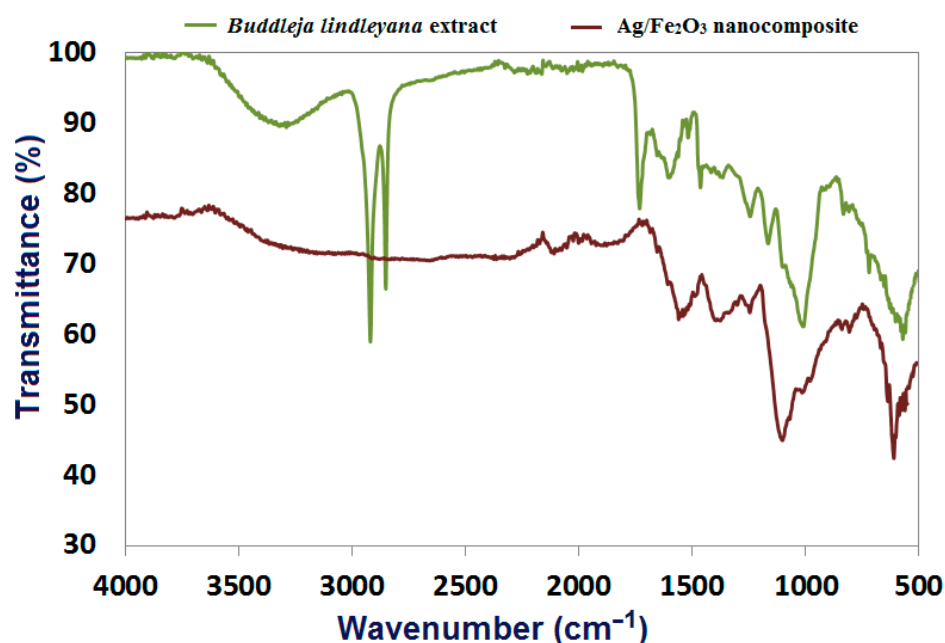
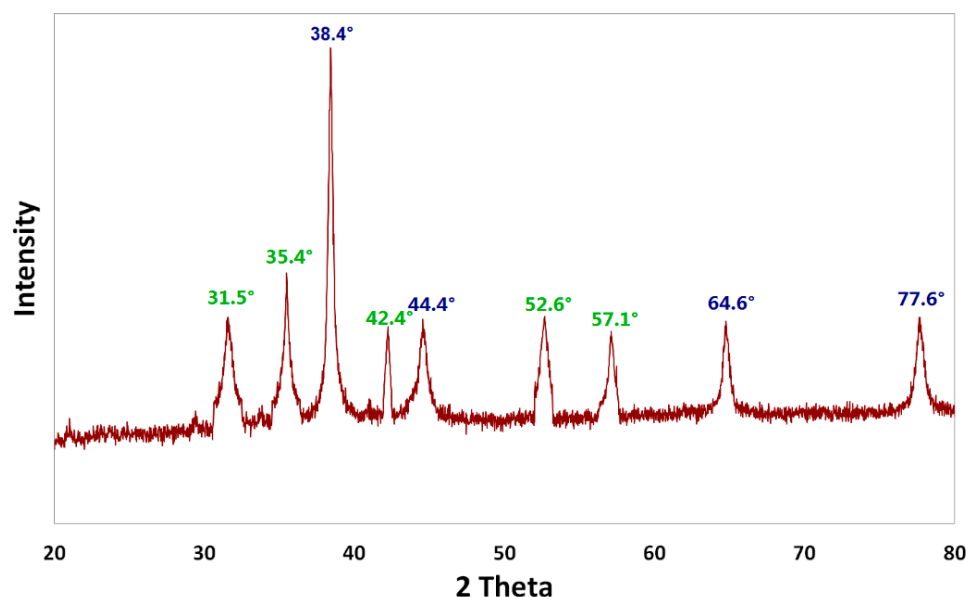


Figure 3. FTIR spectral analysis of *Buddleja lindleyana* extract and Ag/Fe<sub>2</sub>O<sub>3</sub> nanocomposite.

### 3.2. Crystalline Structure of Ag/Fe<sub>2</sub>O<sub>3</sub> Nanoparticles

The crystalline structure of the Ag/Fe<sub>2</sub>O<sub>3</sub> NPs prepared was validated using XRD analysis, as shown in Figure 4. The primary strong angles in the diffractogram of the photosynthesized Ag/Fe<sub>2</sub>O<sub>3</sub> were visible in the XRD patterns, showing that the Ag/Fe<sub>2</sub>O<sub>3</sub> nanocomposite was crystallographic in nature. Bands at  $31.5^\circ$ ,  $35.4^\circ$ ,  $38.4^\circ$ ,  $42.4^\circ$ ,  $44.4^\circ$ ,  $52.6^\circ$ ,  $57.1^\circ$ ,  $64.6^\circ$ , and  $77.6^\circ$  corresponded to Ag/Fe<sub>2</sub>O<sub>3</sub> diffraction peaks. The values of silver appeared at the angles  $38.4^\circ$ ,  $44.4^\circ$ ,  $64.6^\circ$ , and  $77.6^\circ$  [20], while the peaks of the angles for iron oxide appeared at  $31.5^\circ$ ,  $35.4^\circ$ ,  $42.4^\circ$ ,  $52.6^\circ$ , and  $57.1^\circ$  [31]. Therefore, the results clearly support the successful synthesis of nano Ag/Fe<sub>2</sub>O<sub>3</sub>. Diffraction patterns of the Ag/Fe<sub>2</sub>O<sub>3</sub> nanocomposite did not show the presence of any contaminants, which verifies the purity of the Ag/Fe<sub>2</sub>O<sub>3</sub> nanocomposite obtained.



**Figure 4.** X-ray diffraction (XRD) of the Ag/Fe<sub>2</sub>O<sub>3</sub> synthesized by *Buddleja lindleyana* extract.

The most widely used technique for determining the morphological features and sizes of nanostructures is the transmission electron microscope (TEM). Ag/Fe<sub>2</sub>O<sub>3</sub> nanocomposites have been created in various forms such as triangular and spherical with an average size range of 25–174 nm, as seen in the TEM image (Figure 5A). These different forms are a representation of the majority of nanocomposites found in Ag and Fe<sub>2</sub>O<sub>3</sub>. The planes of the nanocomposite, as well as the degree of crystallinity of *Buddleja lindleyana* Ag/Fe<sub>2</sub>O<sub>3</sub> particles, are shown by the bright circular areas in the SAED (selected area electron diffraction) pattern (Figure 5B). The SAED pattern's ring patterns match the Fe<sub>2</sub>O<sub>3</sub> NPs' (104), (110), (113), (024), and (122) planes [70]. The SAED pattern further displays planes (100), (200), (220) and (311) that correspond to silver nanoparticles in addition to the aforementioned planes [71]. The average diameter of the Ag/Fe<sub>2</sub>O<sub>3</sub> nanocomposite was determined using dynamic light scattering (DLS) analysis. The produced Ag/Fe<sub>2</sub>O<sub>3</sub> nanocomposites were a poly-dispersed aggregate with an average diameter of 270.9 nm (Figure 5C). However, biomaterials deposited on the Ag/Fe<sub>2</sub>O<sub>3</sub> surface by *Buddleja lindleyana*, such as organic compounds associated as stabilizers, as well as the metal core (Ag and Fe) of the Ag/Fe<sub>2</sub>O<sub>3</sub> nanocomposite, alter the size determined by DLS [40,72].

SEM was used to analyze the morphology of Ag/Fe<sub>2</sub>O<sub>3</sub> prepared using a simple and single-step process, as demonstrated in Figure 6A. The Ag/Fe<sub>2</sub>O<sub>3</sub> seemed to have a mono-dispersed and aggregation-free micrograph. The EDX spectra revealed the existence of several well-defined peaks in the Ag/Fe<sub>2</sub>O<sub>3</sub> nanocomposite that were due to silver, iron, oxygen, and carbon components (Figure 6B). Furthermore, EDX spectra revealed the production of a very pure Ag/Fe<sub>2</sub>O<sub>3</sub> nanocomposite with no additional impurity-related peaks. The SEM image and the EDX spectra of the nanocomposite prepared revealed that the Ag/Fe<sub>2</sub>O<sub>3</sub> nanostructures were well distributed in the *Buddleja lindleyana* extract [73]. In addition, elemental EDX mapping was used to determine the Ag and Fe elemental distribution (spatial/lateral) of the Ag/Fe<sub>2</sub>O<sub>3</sub> nanocomposite prepared. The mapping of Fe, Ag, O, and C elements can be seen in the picture (Figure 6C). Both Fe and Ag were uniformly distributed throughout the Ag/Fe<sub>2</sub>O<sub>3</sub> sample, according to the EDX elemental analysis shown in the Ag, Fe, O, and C element mapping images of Ag/Fe<sub>2</sub>O<sub>3</sub> (Figure 6) [41].

### 3.3. Antimicrobial Activity

Recently, several pathogenic microorganisms have developed resistance to currently available commercial antibiotic agents and also caused adverse impact on human health. Thus, new active and safe antimicrobial agents are required. Because nanomaterials have

antibacterial capabilities, they have recently received attention [74,75]. According to Figure 7, the well diffusion technique was used in this investigation to evaluate the Ag/Fe<sub>2</sub>O<sub>3</sub> nanocomposite's antibacterial efficacy against human bacterial pathogens (*S aureus*, *E. coli*, *B subtilis*, and *P. aeruginosa*). The maximal Ag/Fe<sub>2</sub>O<sub>3</sub> dose (5 g/mL) showed a high level of inhibitory activity against the pathogens *B. subtilis*, *S. aureus*, *E. coli*, and *P. aeruginosa* with inhibition zones of  $23.4 \pm 0.75$ ,  $22.3 \pm 0.57$ ,  $20.8 \pm 1.6$  and  $19.5 \pm 0.5$  mm, respectively (Figure 7). A previous study showed that silver particles have a good antimicrobial effect on harmful bacteria, whether they are Gram-positive or Gram-negative bacteria [43]. The antibacterial activity of Ag/Fe<sub>2</sub>O<sub>3</sub> nanocomposite was investigated in earlier investigations, and it showed good activity against Gram-negative and Gram-positive bacteria [34,40,76]. Ag/Fe<sub>2</sub>O<sub>3</sub> has an antibacterial impact on bacteria because it damages cell walls, disrupts structural proteins, inactivates enzymes, inhibits electron transport chains, damages nucleic acids (DNA), and causes oxidative stress brought on by the generation of reactive oxygen species (ROS) [41,72,77]. As a result, Ag/Fe<sub>2</sub>O<sub>3</sub> has emerged as a viable antibacterial treatment option and is useful in the medicinal field.

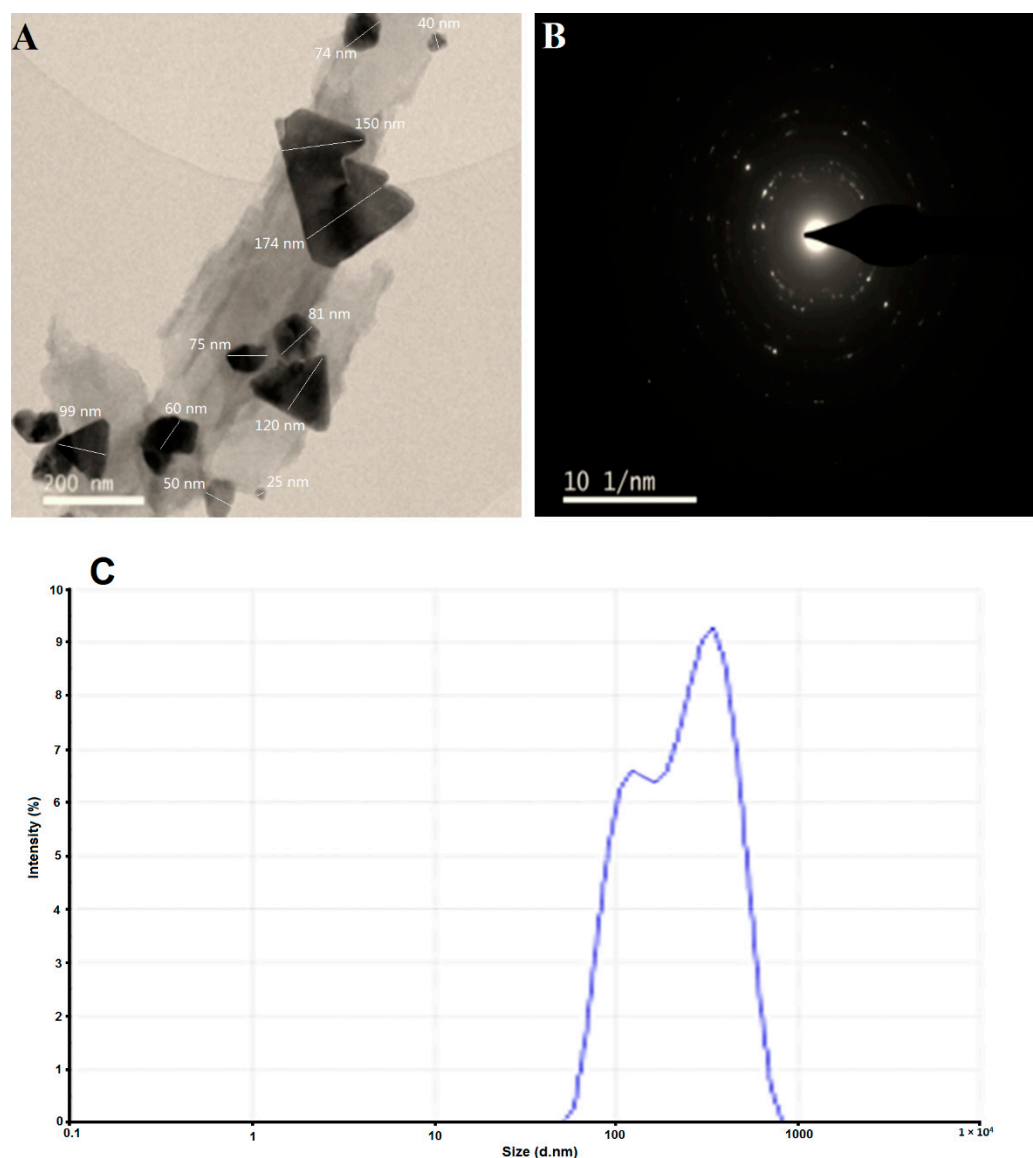


**Figure 5.** TEM image (A), SAED pattern (B), and DLS (C) of the synthesized Ag/Fe<sub>2</sub>O<sub>3</sub> by *Buddleja lindleyana* extract.

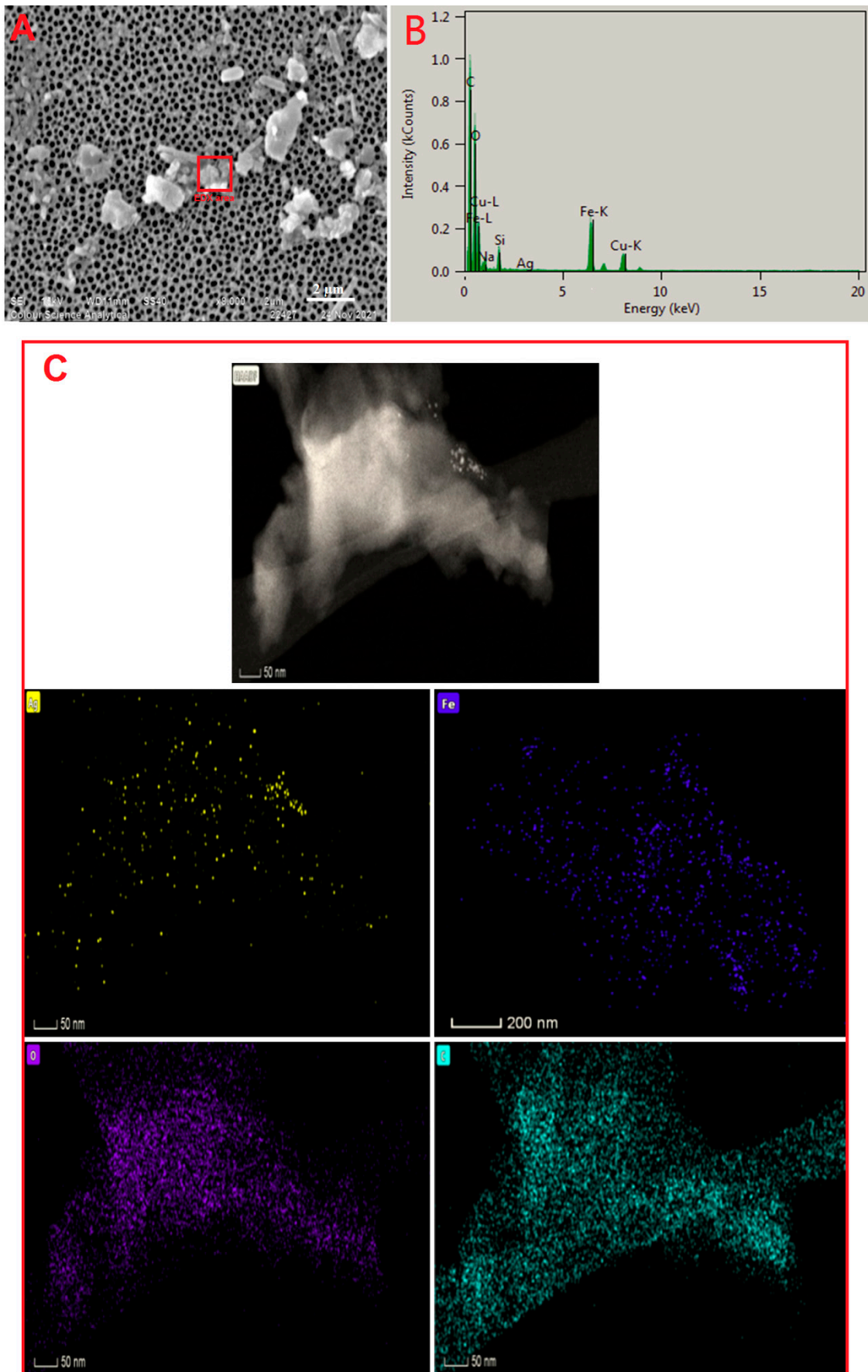
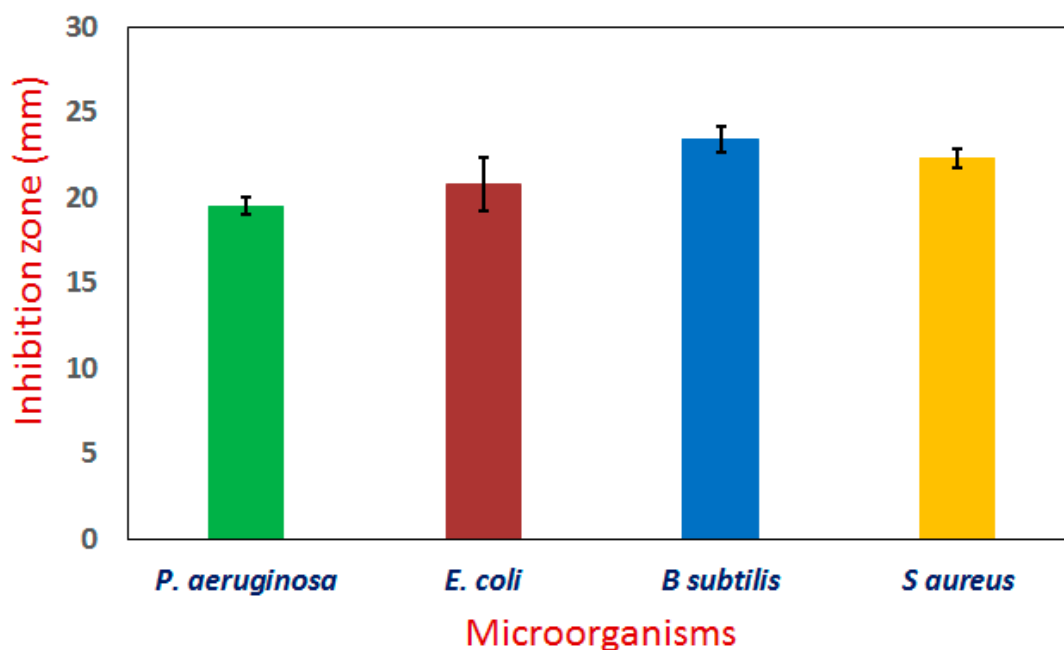


Figure 6. (A) SEM image, (B) EDX spectrum, and (C) element mapping of Ag/Fe<sub>2</sub>O<sub>3</sub> nanocomposites.



**Figure 7.** Antimicrobial activity of the synthesized Ag/Fe<sub>2</sub>O<sub>3</sub> by *Buddleja lindleyana* extract.

#### 4. Conclusions

*Buddleja lindleyana* extract was used for the phytosynthesis of Ag/Fe<sub>2</sub>O<sub>3</sub>NP through an eco-friendly route. The fabricated Ag/Fe<sub>2</sub>O<sub>3</sub> nanocomposites were characterized using UV-Vis, FTIR, XRD, TEM, DLS and SEM-EDX analyses. The Ag/Fe<sub>2</sub>O<sub>3</sub> nanocomposites obtained are triangular–spheroidal and exhibit a high absorbance band around 320 nm. According to the observation made from the FTIR analysis, it is possible to conclude that the compounds present in *Buddleja lindleyana*'s extract play an important role in the reduction and stabilization of nanocomposites. The Ag/Fe<sub>2</sub>O<sub>3</sub>NPs obtained are stable in colloidal solution. Results also revealed that the Ag/Fe<sub>2</sub>O<sub>3</sub>NP nanocomposites fabricated have outstanding antimicrobial activity against pathogenic strains (*S. aureus*, *E. coli*, *B. subtilis*, and *P. aeruginosa*). It was found that the antimicrobial activity of the Ag/Fe<sub>2</sub>O<sub>3</sub> nanocomposites is dependent on the structure of the nanocomposites, which have significant activity against all bacterial strains tested. Finally, the Ag/Fe<sub>2</sub>O<sub>3</sub> nanocomposites biosynthesized using the extract of *Buddleja lindleyana* were also shown to have antibacterial properties, making them promising materials for usage in the medical field.

**Author Contributions:** Conceptualization, F.A.M.A.-Z. and R.M.E.-S.; methodology, F.A.M.A.-Z., S.S.S. and R.M.E.-S.; software, S.S.S.; validation, L.L.; formal analysis, S.S.S., H.A.A.-G., L.M.N. and L.L.; investigation, F.A.M.A.-Z., S.S.S., H.A.A.-G., L.M.N. and L.L.; resources, L.L.; data curation, H.A.A.-G., L.M.N. and L.L.; writing—original draft preparation, F.A.M.A.-Z. and S.S.S.; writing—review and editing, F.A.M.A.-Z., S.S.S., H.A.A.-G., L.M.N., L.L. and R.M.E.-S.; visualization, R.M.E.-S.; funding acquisition, F.A.M.A.-Z. All authors have read and agreed to the published version of the manuscript.

**Funding:** Small Groups Project under grant number (RGP.1/252/43) Deanship of Scientific Research at King Khalid University.

**Institutional Review Board Statement:** Not applicable.

**Informed Consent Statement:** Not applicable.

**Data Availability Statement:** The data used to support the findings of this study are available from the corresponding author upon request.

**Acknowledgments:** The authors extend their appreciation to the Scientific Research at King Khalid University for funding this work through Small Groups Project under grant number (RGP.1/252/43).

**Conflicts of Interest:** The authors declare no conflict of interest.

## References

1. Hassanisaadi, M.; Bonjar, A.H.S.; Rahdar, A.; Varma, R.S.; Ajalli, N.; Pandey, S. Eco-friendly biosynthesis of silver nanoparticles using *Aloysia citrodora* leaf extract and evaluations of their bioactivities. *Mater. Today Commun.* **2022**, *33*, 104183. [[CrossRef](#)]
2. Perveen, S.; Nadeem, R.; Rehman, S.u.; Afzal, N.; Anjum, S.; Noreen, S.; Saeed, R.; Amami, M.; Al-Mijalli, S.H.; Iqbal, M. Green synthesis of iron (Fe) nanoparticles using *Plumeria obtusa* extract as a reducing and stabilizing agent: Antimicrobial, antioxidant and biocompatibility studies. *Arab. J. Chem.* **2022**, *15*, 103764. [[CrossRef](#)]
3. Narath, S.; Koroth, S.K.; Shankar, S.S.; George, B.; Mutta, V.; Wacławek, S.; Černík, M.; Padil, V.V.T.; Varma, R.S. Cinnamomum tamala leaf extract stabilized zinc oxide nanoparticles: A promising photocatalyst for methylene blue degradation. *Nanomaterials* **2021**, *11*, 1558. [[CrossRef](#)]
4. Hashem, A.H.; Salem, S.S. Green and ecofriendly biosynthesis of selenium nanoparticles using *Urtica dioica* (stinging nettle) leaf extract: Antimicrobial and anticancer activity. *Biotechnol. J.* **2022**, *17*, 2100432. [[CrossRef](#)]
5. Haydar, M.S.; Das, D.; Ghosh, S.; Mandal, P. Implementation of mature tea leaves extract in bioinspired synthesis of iron oxide nanoparticles: Preparation, process optimization, characterization, and assessment of therapeutic potential. *Chem. Pap.* **2022**, *76*, 491–514. [[CrossRef](#)]
6. Singh, R.; Hano, C.; Nath, G.; Sharma, B. Green Biosynthesis of Silver Nanoparticles Using Leaf Extract of *Carissa carandas* L. and Their Antioxidant and Antimicrobial Activity against Human Pathogenic Bacteria. *Biomolecules* **2021**, *11*, 299. [[CrossRef](#)]
7. Mareedu, T.; Poiba, V.; Vangalapati, M. Green synthesis of iron nanoparticles by green tea and black tea leaves extract. *Mater. Today Proc.* **2021**, *42*, 1498–1501. [[CrossRef](#)]
8. Salem, S.S.; Hammad, E.N.; Mohamed, A.A.; El-Dougdoug, W. A Comprehensive Review of Nanomaterials: Types, Synthesis, Characterization, and Applications. *Biointerface Res. Appl. Chem.* **2022**, *13*, 41. [[CrossRef](#)]
9. Eid, A.M.; Fouda, A.; Niedbala, G.; Hassan, S.E.D.; Salem, S.S.; Abdo, A.M.; Hetta, H.F.; Shaheen, T.I. Endophytic streptomyces laurentii mediated green synthesis of Ag-NPs with antibacterial and anticancer properties for developing functional textile fabric properties. *Antibiotics* **2020**, *9*, 641. [[CrossRef](#)]
10. Salem, S.S. Bio-fabrication of Selenium Nanoparticles Using Baker's Yeast Extract and Its Antimicrobial Efficacy on Food Borne Pathogens. *Appl. Biochem. Biotechnol.* **2022**, *194*, 1898–1910. [[CrossRef](#)]
11. Mohamed, A.A.; Abu-Elghait, M.; Ahmed, N.E.; Salem, S.S. Eco-friendly Mycogenic Synthesis of ZnO and CuO Nanoparticles for In Vitro Antibacterial, Antibiofilm, and Antifungal Applications. *Biol. Trace Elem. Res.* **2021**, *199*, 2788–2799. [[CrossRef](#)]
12. Salem, S.S.; Fouda, A. Green Synthesis of Metallic Nanoparticles and Their Prospective Biotechnological Applications: An Overview. *Biol. Trace Elem. Res.* **2021**, *199*, 344–370. [[CrossRef](#)]
13. Badawy, A.A.; Abdelfattah, N.A.H.; Salem, S.S.; Awad, M.F.; Fouda, A. Efficacy assessment of biosynthesized copper oxide nanoparticles (CuO-nps) on stored grain insects and their impacts on morphological and physiological traits of wheat (*Triticum aestivum* L.) plant. *Biology* **2021**, *10*, 233. [[CrossRef](#)]
14. Salem, S.S.; Husen, A. Chapter 14—Effect of engineered nanomaterials on soil microbiomes and their association with crop growth and production. In *Engineered Nanomaterials for Sustainable Agricultural Production, Soil Improvement and Stress Management*; Husen, A., Ed.; Academic Press: Cambridge, MA, USA, 2022; pp. 311–336.
15. Hashem, A.H.; Shehabeldine, A.M.; Ali, O.M.; Salem, S.S. Synthesis of Chitosan-Based Gold Nanoparticles: Antimicrobial and Wound-Healing Activities. *Polymers* **2022**, *14*, 2293. [[CrossRef](#)]
16. Abdelaziz, A.M.; Salem, S.S.; Khalil, A.M.A.; El-Wakil, D.A.; Fouda, H.M.; Hashem, A.H. Potential of biosynthesized zinc oxide nanoparticles to control Fusarium wilt disease in eggplant (*Solanum melongena*) and promote plant growth. *BioMetals* **2022**, *35*, 601–616. [[CrossRef](#)]
17. Shaheen, T.I.; Salem, S.S.; Fouda, A. Current Advances in Fungal Nanobiotechnology: Mycofabrication and Applications. In *Microbial Nanobiotechnology: Principles and Applications*; Lateef, A., Gueguim-Kana, E.B., Dasgupta, N., Ranjan, S., Eds.; Springer: Singapore, 2021; pp. 113–143.
18. Mohamed, A.A.; Fouda, A.; Abdel-Rahman, M.A.; Hassan, S.E.D.; El-Gamal, M.S.; Salem, S.S.; Shaheen, T.I. Fungal strain impacts the shape, bioactivity and multifunctional properties of green synthesized zinc oxide nanoparticles. *Biocatal. Agric. Biotechnol.* **2019**, *19*, 101103. [[CrossRef](#)]
19. Shaheen, T.I.; Fouda, A.; Salem, S.S. Integration of Cotton Fabrics with Biosynthesized CuO Nanoparticles for Bactericidal Activity in the Terms of Their Cytotoxicity Assessment. *Ind. Eng. Chem. Res.* **2021**, *60*, 1553–1563. [[CrossRef](#)]
20. Al-Rajhi, A.M.H.; Salem, S.S.; Alharbi, A.A.; Abdelghany, T.M. Ecofriendly synthesis of silver nanoparticles using Kei-apple (*Dovyalis caffra*) fruit and their efficacy against cancer cells and clinical pathogenic microorganisms. *Arab. J. Chem.* **2022**, *15*, 103927. [[CrossRef](#)]
21. Hammad, E.N.; Salem, S.S.; Zohair, M.M.; Mohamed, A.A.; El-Dougdoug, W. Purpureocillium lilacinum mediated biosynthesis copper oxide nanoparticles with promising removal of dyes. *Biointerface Res. Appl. Chem.* **2022**, *12*, 1397–1404. [[CrossRef](#)]
22. Fouda, A.; Salem, S.S.; Wassel, A.R.; Hamza, M.F.; Shaheen, T.I. Optimization of green biosynthesized visible light active CuO/ZnO nano-photocatalysts for the degradation of organic methylene blue dye. *Heliyon* **2020**, *6*, e04896. [[CrossRef](#)]

23. Hashem, A.H.; Selim, T.A.; Alruhaili, M.H.; Selim, S.; Alkhalifah, D.H.M.; Al Jaouni, S.K.; Salem, S.S. Unveiling Antimicrobial and Insecticidal Activities of Biosynthesized Selenium Nanoparticles Using Prickly Pear Peel Waste. *J. Funct. Biomater.* **2022**, *13*, 112. [[CrossRef](#)]
24. Salem, S.S.; Badawy, M.S.E.M.; Al-Askar, A.A.; Arishi, A.A.; Elkady, F.M.; Hashem, A.H. Green Biosynthesis of Selenium Nanoparticles Using Orange Peel Waste: Characterization, Antibacterial and Antibiofilm Activities against Multidrug-Resistant Bacteria. *Life* **2022**, *12*, 893. [[CrossRef](#)]
25. Sharaf, M.H.; Nagiub, A.M.; Salem, S.S.; Kalaba, M.H.; El Fakharany, E.M.; Abd El-Wahab, H. A new strategy to integrate silver nanowires with waterborne coating to improve their antimicrobial and antiviral properties. *Pigment Resin Technol.* **2022**. *ahead-of-print*. [[CrossRef](#)]
26. Shehabeldine, A.M.; Salem, S.S.; Ali, O.M.; Abd-Elsalam, K.A.; Elkady, F.M.; Hashem, A.H. Multifunctional Silver Nanoparticles Based on Chitosan: Antibacterial, Antibiofilm, Antifungal, Antioxidant, and Wound-Healing Activities. *J. Fungi* **2022**, *8*, 612. [[CrossRef](#)]
27. Alsharif, S.M.; Salem, S.S.; Abdel-Rahman, M.A.; Fouda, A.; Eid, A.M.; El-Din Hassan, S.; Awad, M.A.; Mohamed, A.A. Multifunctional properties of spherical silver nanoparticles fabricated by different microbial taxa. *Heliyon* **2020**, *6*, e03943. [[CrossRef](#)]
28. Salem, S.S.; El-Belely, E.F.; Niedbała, G.; Alnoman, M.M.; Hassan, S.E.D.; Eid, A.M.; Shaheen, T.I.; Elkelish, A.; Fouda, A. Bactericidal and in-vitro cytotoxic efficacy of silver nanoparticles (Ag-NPs) fabricated by endophytic actinomycetes and their use as coating for the textile fabrics. *Nanomaterials* **2020**, *10*, 2082. [[CrossRef](#)]
29. Abdallah, B.M.; Ali, E.M. Green Synthesis of Silver Nanoparticles Using the Lotus lalambensis Aqueous Leaf Extract and Their Anti-Candidal Activity against Oral Candidiasis. *ACS Omega* **2021**, *6*, 8151–8162. [[CrossRef](#)]
30. Salem, S.S. Baker's Yeast-Mediated Silver Nanoparticles: Characterisation and Antimicrobial Biogenic Tool for Suppressing Pathogenic Microbes. *BioNanoScience* **2022**. [[CrossRef](#)]
31. Kulkarni, S.; Jadhav, M.; Raikar, P.; Barretto, D.A.; Vootla, S.K.; Raikar, U.S. Green synthesized multifunctional Ag@Fe<sub>2</sub>O<sub>3</sub> nanocomposites for effective antibacterial, antifungal and anticancer properties. *New J. Chem.* **2017**, *41*, 9513–9520. [[CrossRef](#)]
32. Ansari, M.A.; Asiri, S.M.M. Green synthesis, antimicrobial, antibiofilm and antitumor activities of superparamagnetic  $\gamma$ -Fe<sub>2</sub>O<sub>3</sub> NPs and their molecular docking study with cell wall mannoproteins and peptidoglycan. *Int. J. Biol. Macromol.* **2021**, *171*, 44–58. [[CrossRef](#)]
33. Demarchi, C.A.; Bella Cruz, A.; Ślawska-Waniewska, A.; Nedelko, N.; Dłużewski, P.; Kaleta, A.; Trzciński, J.; Magro, J.D.; Scapinello, J.; Rodrigues, C.A. Synthesis of Ag@Fe<sub>2</sub>O<sub>3</sub> nanocomposite based on O-carboxymethylchitosan with antimicrobial activity. *Int. J. Biol. Macromol.* **2018**, *107*, 42–51. [[CrossRef](#)]
34. Gao, N.; Chen, Y.; Jiang, J. Ag@Fe<sub>2</sub>O<sub>3</sub>-GO Nanocomposites Prepared by a Phase Transfer Method with Long-Term Antibacterial Property. *ACS Appl. Mater. Interfaces* **2013**, *5*, 11307–11314. [[CrossRef](#)]
35. Shahriary, M.; Veisi, H.; Hekmati, M.; Hemmati, S. In situ green synthesis of Ag nanoparticles on herbal tea extract (*Stachys lavandulifolia*)-modified magnetic iron oxide nanoparticles as antibacterial agent and their 4-nitrophenol catalytic reduction activity. *Mater. Sci. Eng. C* **2018**, *90*, 57–66. [[CrossRef](#)]
36. Chen, D.; Jiang, M.; Li, N.; Gu, H.; Xu, Q.; Ge, J.; Xia, X.; Lu, J. Modification of magnetic silica/iron oxide nanocomposites with fluorescent polymethacrylic acid for cancer targeting and drug delivery. *J. Mater. Chem.* **2010**, *20*, 6422–6429. [[CrossRef](#)]
37. Li, Y.; Wang, Z.; Liu, R. Superparamagnetic  $\alpha$ -Fe<sub>2</sub>O<sub>3</sub>/Fe<sub>3</sub>O<sub>4</sub> Heterogeneous Nanoparticles with Enhanced Biocompatibility. *Nanomaterials* **2021**, *11*, 834. [[CrossRef](#)] [[PubMed](#)]
38. Kaloti, M.; Kumar, A. Sustainable Catalytic Activity of Ag-Coated Chitosan-Capped  $\gamma$ -Fe<sub>2</sub>O<sub>3</sub> Superparamagnetic Binary Nanohybrids (Ag- $\gamma$ -Fe<sub>2</sub>O<sub>3</sub>@CS) for the Reduction of Environmentally Hazardous Dyes—A Kinetic Study of the Operating Mechanism Analyzing Methyl Orange Reduction. *ACS Omega* **2018**, *3*, 1529–1545. [[CrossRef](#)]
39. Fernández-Barahona, I.; Muñoz-Hernando, M.; Ruiz-Cabello, J.; Herranz, F.; Pellico, J. Iron Oxide Nanoparticles: An Alternative for Positive Contrast in Magnetic Resonance Imaging. *Inorganics* **2020**, *8*, 28. [[CrossRef](#)]
40. Luengo, Y.; Sot, B.; Salas, G. Combining Ag and  $\gamma$ -Fe<sub>2</sub>O<sub>3</sub> properties to produce effective antibacterial nanocomposites. *Colloids Surf. B Biointerfaces* **2020**, *194*, 111178. [[CrossRef](#)]
41. Khan, A.U.; Rahman, A.u.; Yuan, Q.; Ahmad, A.; Khan, Z.U.H.; Mahnashi, M.H.; Alyami, B.A.; Alqahtani, Y.S.; Ullah, S.; Wirman, A.P. Facile and eco-benign fabrication of Ag/Fe<sub>2</sub>O<sub>3</sub> nanocomposite using *Algaia Monozyga* leaves extract and its' efficient biocidal and photocatalytic applications. *Photodiagnosis Photodyn. Ther.* **2020**, *32*, 101970. [[CrossRef](#)]
42. Kaloti, M.; Kumar, A.; Navani, N.K. Synthesis of glucose-mediated Ag- $\gamma$ -Fe<sub>2</sub>O<sub>3</sub> multifunctional nanocomposites in aqueous medium—A kinetic analysis of their catalytic activity for 4-nitrophenol reduction. *Green Chem.* **2015**, *17*, 4786–4799. [[CrossRef](#)]
43. Chen, Y.; Gao, N.; Jiang, J. Surface Matters: Enhanced Bactericidal Property of Core-Shell Ag-Fe<sub>2</sub>O<sub>3</sub> Nanostructures to Their Heteromer Counterparts from One-Pot Synthesis. *Small* **2013**, *9*, 3242–3246. [[CrossRef](#)] [[PubMed](#)]
44. Shaheen, T.I.; Salem, S.S.; Zaghloul, S. A New Facile Strategy for Multifunctional Textiles Development through in Situ Deposition of SiO<sub>2</sub>/TiO<sub>2</sub> Nanosols Hybrid. *Ind. Eng. Chem. Res.* **2019**, *58*, 20203–20212. [[CrossRef](#)]
45. Elfeky, A.S.; Salem, S.S.; Elzaref, A.S.; Owda, M.E.; Eladawy, H.A.; Saeed, A.M.; Awad, M.A.; Abou-Zeid, R.E.; Fouda, A. Multifunctional cellulose nanocrystal /metal oxide hybrid, photo-degradation, antibacterial and larvicidal activities. *Carbohydr. Polym.* **2020**, *230*, 115711. [[CrossRef](#)]

46. Abu-Elghait, M.; Hasanin, M.; Hashem, A.H.; Salem, S.S. Ecofriendly novel synthesis of tertiary composite based on cellulose and myco-synthesized selenium nanoparticles: Characterization, antibiofilm and biocompatibility. *Int. J. Biol. Macromol.* **2021**, *175*, 294–303. [[CrossRef](#)]
47. Abdelmoneim, H.E.M.; Wassel, M.A.; Elfeky, A.S.; Bendary, S.H.; Awad, M.A.; Salem, S.S.; Mahmoud, S.A. Multiple Applications of CdS/TiO<sub>2</sub> Nanocomposites Synthesized via Microwave-Assisted Sol–Gel. *J. Clust. Sci.* **2022**, *33*, 1119–1128. [[CrossRef](#)]
48. Smuleac, V.; Varma, R.; Baruwati, B.; Sikdar, S.; Bhattacharyya, D. Nanostructured Membranes for Enzyme Catalysis and Green Synthesis of Nanoparticles. *ChemSusChem* **2011**, *4*, 1773–1777. [[CrossRef](#)]
49. Smuleac, V.; Varma, R.; Sikdar, S.; Bhattacharyya, D. Green synthesis of Fe and Fe/Pd bimetallic nanoparticles in membranes for reductive degradation of chlorinated organics. *J. Membr. Sci.* **2011**, *379*, 131–137. [[CrossRef](#)]
50. Plachtová, P.; Medříková, Z.; Zbořil, R.; Tuček, J.; Varma, R.S.; Maršálek, B. Iron and Iron Oxide Nanoparticles Synthesized with Green Tea Extract: Differences in Ecotoxicological Profile and Ability To Degrade Malachite Green. *ACS Sustain. Chem. Eng.* **2018**, *6*, 8679–8687. [[CrossRef](#)]
51. Markova, Z.; Novak, P.; Kaslik, J.; Plachtova, P.; Brazdova, M.; Jancula, D.; Siskova, K.M.; Machala, L.; Marsalek, B.; Zboril, R.; et al. Iron(II,III)–Polyphenol Complex Nanoparticles Derived from Green Tea with Remarkable Ecotoxicological Impact. *ACS Sustain. Chem. Eng.* **2014**, *2*, 1674–1680. [[CrossRef](#)]
52. Saied, E.; Eid, A.M.; Hassan, S.E.D.; Salem, S.S.; Radwan, A.A.; Halawa, M.; Saleh, F.M.; Saad, H.A.; Saied, E.M.; Fouda, A. The catalytic activity of biosynthesized magnesium oxide nanoparticles (Mgo-nps) for inhibiting the growth of pathogenic microbes, tanning effluent treatment, and chromium ion removal. *Catalysts* **2021**, *11*, 821. [[CrossRef](#)]
53. Hashem, A.H.; Khalil, A.M.A.; Reyad, A.M.; Salem, S.S. Biomedical Applications of Mycosynthesized Selenium Nanoparticles Using *Penicillium expansum* ATTC 36200. *Biol. Trace Elem. Res.* **2021**, *199*, 3998–4008. [[CrossRef](#)] [[PubMed](#)]
54. Salem, S.S.; Fouda, M.M.G.; Fouda, A.; Awad, M.A.; Al-Olayan, E.M.; Allam, A.A.; Shaheen, T.I. Antibacterial, Cytotoxicity and Larvicidal Activity of Green Synthesized Selenium Nanoparticles Using *Penicillium corylophilum*. *J. Clust. Sci.* **2021**, *32*, 351–361. [[CrossRef](#)]
55. Mohmed, A.A.; Fouda, A.; Elgamal, M.S.; El-Din Hassan, S.; Shaheen, T.I.; Salem, S.S. Enhancing of cotton fabric antibacterial properties by silver nanoparticles synthesized by new egyptian strain *Fusarium keratoplasticum* A1-3. *Egypt. J. Chem.* **2017**, *60*, 63–71. [[CrossRef](#)]
56. Mohammadzadeh, V.; Barani, M.; Amiri, M.S.; Taghavizadeh Yazdi, M.E.; Hassanisaadi, M.; Rahdar, A.; Varma, R.S. Applications of plant-based nanoparticles in nanomedicine: A review. *Sustain. Chem. Pharm.* **2022**, *25*, 100606. [[CrossRef](#)]
57. Nadagouda, M.N.; Castle, A.B.; Murdock, R.C.; Hussain, S.M.; Varma, R.S. In vitro biocompatibility of nanoscale zerovalent iron particles (NZVI) synthesized using tea polyphenols. *Green Chem.* **2010**, *12*, 114–122. [[CrossRef](#)]
58. Makarov, V.V.; Makarova, S.S.; Love, A.J.; Sinitsyna, O.V.; Dudnik, A.O.; Yaminsky, I.V.; Taliany, M.E.; Kalinina, N.O. Biosynthesis of Stable Iron Oxide Nanoparticles in Aqueous Extracts of *Hordeum vulgare* and *Rumex acetosa* Plants. *Langmuir* **2014**, *30*, 5982–5988. [[CrossRef](#)]
59. Sharma, J.K.; Srivastava, P.; Akhtar, M.S.; Singh, G.; Ameen, S.  $\alpha$ -Fe<sub>2</sub>O<sub>3</sub> hexagonal cones synthesized from the leaf extract of *Azadirachta indica* and its thermal catalytic activity. *New J. Chem.* **2015**, *39*, 7105–7111. [[CrossRef](#)]
60. Mohamed, H.E.A.; Afridi, S.; Khalil, A.T.; Ali, M.; Zohra, T.; Salman, M.; Ikram, A.; Shinwari, Z.K.; Maaza, M. Bio-redox potential of *Hyphaene thebaica* in bio-fabrication of ultrafine maghemite phase iron oxide nanoparticles (Fe<sub>2</sub>O<sub>3</sub> NPs) for therapeutic applications. *Mater. Sci. Eng. C* **2020**, *112*, 110890. [[CrossRef](#)]
61. Alangari, A.; Alqahtani, M.S.; Mateen, A.; Kalam, M.A.; Alshememry, A.; Ali, R.; Kazi, M.; AlGhamdi, K.M.; Syed, R. Iron Oxide Nanoparticles: Preparation, Characterization, and Assessment of Antimicrobial and Anticancer Activity. *Adsorpt. Sci. Technol.* **2022**, *2022*, 1562051. [[CrossRef](#)]
62. Saied, E.; Salem, S.S.; Al-Askar, A.A.; Elkady, F.M.; Arishi, A.A.; Hashem, A.H. Mycosynthesis of Hematite ( $\alpha$ -Fe<sub>2</sub>O<sub>3</sub>) Nanoparticles Using *Aspergillus niger* and Their Antimicrobial and Photocatalytic Activities. *Bioengineering* **2022**, *9*, 397. [[CrossRef](#)]
63. Hammad, E.N.; Salem, S.S.; Mohamed, A.A.; El-DougDoug, W. Environmental Impacts of Ecofriendly Iron Oxide Nanoparticles on Dyes Removal and Antibacterial Activity. *Appl. Biochem. Biotechnol.* **2022**. [[CrossRef](#)] [[PubMed](#)]
64. Wu, D.-L.; Wang, Y.-K.; Liu, J.-S.; Wang, X.-C.; Zhang, W. Two new compounds from the fruits of *Buddleja lindleyana* with neuroprotective effect. *J. Asian Nat. Prod. Res.* **2012**, *14*, 342–347. [[CrossRef](#)] [[PubMed](#)]
65. Tai, B.H.; Nhiem, N.X.; Quang, T.H.; Ngan, N.T.T.; Tung, N.H.; Kim, Y.; Lee, J.-J.; Myung, C.-S.; Cuong, N.M.; Kim, Y.H. A new iridoid and effect on the rat aortic vascular smooth muscle cell proliferation of isolated compounds from *Buddleja officinalis*. *Bioorganic Med. Chem. Lett.* **2011**, *21*, 3462–3466. [[CrossRef](#)]
66. Lu, J.-H.; Pu, X.-P.; Li, Y.-Y.; Zhao, Y.-Y.; Tu, G.-Z. Bioactive Phenylethanoid Glycosides from *Buddleja lindleyana*. *Z. Für Nat. B* **2005**, *60*, 211–214. [[CrossRef](#)]
67. Berastegui, P.; Tai, C.-W.; Valvo, M. Electrochemical reactions of AgFeO<sub>2</sub> as negative electrode in Li- and Na-ion batteries. *J. Power Sources* **2018**, *401*, 386–396. [[CrossRef](#)]
68. Qasim, S.; Zafar, A.; Saif, M.S.; Ali, Z.; Nazar, M.; Waqas, M.; Haq, A.U.; Tariq, T.; Hassan, S.G.; Iqbal, F. Green synthesis of iron oxide nanorods using *Withania coagulans* extract improved photocatalytic degradation and antimicrobial activity. *J. Photochem. Photobiol. B Biol.* **2020**, *204*, 111784. [[CrossRef](#)]
69. Espenti, C.S.; Rao, K.K.; Rao, K.M. Bio-synthesis and characterization of silver nanoparticles using *Terminalia chebula* leaf extract and evaluation of its antimicrobial potential. *Mater. Lett.* **2016**, *174*, 129–133. [[CrossRef](#)]

70. Huang, Y.; Ding, D.; Zhu, M.; Meng, W.; Huang, Y.; Geng, F.; Li, J.; Lin, J.; Tang, C.; Lei, Z.; et al. Facile synthesis of  $\alpha$ -Fe<sub>2</sub>O<sub>3</sub> nanodisk with superior photocatalytic performance and mechanism insight. *Sci. Technol. Adv. Mater.* **2015**, *16*, 014801. [[CrossRef](#)]
71. Salem, S.S.; Ali, O.M.; Reyad, A.M.; Abd-El Salam, K.A.; Hashem, A.H. Pseudomonas indica-Mediated Silver Nanoparticles: Antifungal and Antioxidant Biogenic Tool for Suppressing Mucormycosis Fungi. *J. Fungi* **2022**, *8*, 126. [[CrossRef](#)]
72. Aref, M.S.; Salem, S.S. Bio-callus synthesis of silver nanoparticles, characterization, and antibacterial activities via Cinnamomum camphora callus culture. *Biocatal. Agric. Biotechnol.* **2020**, *27*, 101689. [[CrossRef](#)]
73. Biswal, S.K.; Panigrahi, G.K.; Sahoo, S.K. Green synthesis of Fe<sub>2</sub>O<sub>3</sub>-Ag nanocomposite using Psidium guajava leaf extract: An eco-friendly and recyclable adsorbent for remediation of Cr (VI) from aqueous media. *Biophys. Chem.* **2020**, *263*, 106392. [[CrossRef](#)] [[PubMed](#)]
74. Jia, C.; Guo, Y.; Wu, F.-G. Chemodynamic Therapy via Fenton and Fenton-Like Nanomaterials: Strategies and Recent Advances. *Small* **2022**, *18*, 2103868. [[CrossRef](#)]
75. Salem, S.S.; Hashem, A.H.; Sallam, A.-A.M.; Doghish, A.S.; Al-Askar, A.A.; Arishi, A.A.; Shehabeldine, A.M. Synthesis of Silver Nanocomposite Based on Carboxymethyl Cellulose: Antibacterial, Antifungal and Anticancer Activities. *Polymers* **2022**, *14*, 3352. [[CrossRef](#)]
76. Al-Zahrani, F.A.M.; Al-Zahrani, N.A.; Al-Ghamdi, S.N.; Lin, L.; Salem, S.S.; El-Shishtawy, R.M. Synthesis of Ag/Fe<sub>2</sub>O<sub>3</sub> nanocomposite from essential oil of ginger via green method and its bactericidal activity. *Biomass Convers. Biorefinery* **2022**. [[CrossRef](#)]
77. Wei, Z.; Zhou, Z.; Yang, M.; Lin, C.; Zhao, Z.; Huang, D.; Chen, Z.; Gao, J. Multifunctional Ag@Fe<sub>2</sub>O<sub>3</sub> yolk-shell nanoparticles for simultaneous capture, kill, and removal of pathogen. *J. Mater. Chem.* **2011**, *21*, 16344–16348. [[CrossRef](#)]